

# Student Guides Teacher: Weak-to-Strong Inference via Spectral Orthogonal Exploration

Dayu Wang<sup>1</sup> Jiaye Yang<sup>1</sup> Weikang Li<sup>2</sup> Jiahui Liang<sup>1</sup> Yang Li<sup>1</sup>

<sup>1</sup>Baidu Inc.

<sup>2</sup>Peking University

2100010872@stu.pku.edu.cn yamseyoung@gmail.com

wavejkd@pku.edu.cn {liangjiahui03, liyang164}@baidu.com

## Abstract

While Large Language Models (LLMs) demonstrate near-human capabilities, they often suffer from “Reasoning Collapse” in complex mathematical proving and long-horizon planning. Models tend to degenerate into low-rank **Bias Manifold**, where stochastic sampling merely produces lexical variations of erroneous logic rather than semantic exploration. This geometric collapse renders the model “blind” to high-value solutions that lie within its Null Space. To address this, we propose **Spectral Orthogonal Exploration (SOE)**, a geometric framework operating on a counter-intuitive “Student Guides Teacher” paradigm. Specifically, we utilize a weak auxiliary agent not for imitation, but as an *orthogonal probe*. By explicitly navigating the Teacher’s Null Space, SOE serves as a geometric bridge, effectively ejecting the model from local optima to explore diverse, high-value solution spaces. Experiments on mathematical benchmarks demonstrate that, relative to baseline methods, our approach improves average accuracy by **62.4%** and increases average sampling efficiency by **113.7%**, indicating a promising path toward overcoming performance plateaus in advanced reasoning tasks. The code is available at <https://github.com/dayuwang401/SOE->.

## 1 Introduction

Current Large Language Models (LLMs) exhibit a paradox in complex reasoning: while they demonstrate emergent capabilities driven by scaling laws (Kaplan et al., 2020; Wei et al., 2022; Hoffmann et al., 2022; DeepSeek-AI et al., 2025b,a,c; Bubeck et al., 2025), they frequently encounter a catastrophic failure mode known as *Reasoning Collapse* (Shojaee et al., 2025; Zhao et al., 2025; Guo et al., 2025; Yamin et al., 2025). When facing long-horizon mathematical proofs or logic puzzles, model performance does not decay gracefully but

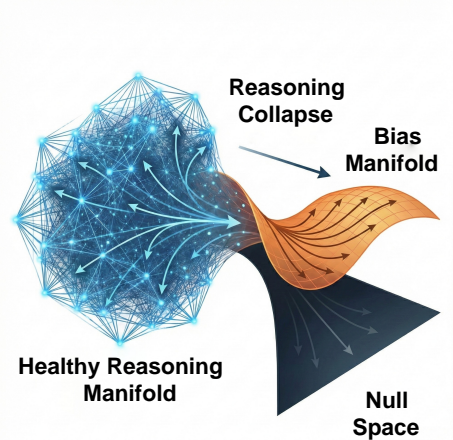


Figure 1: Geometric Interpretation of **Reasoning Collapse**. We characterize reasoning collapse as the transition of the state space from a high-dimensional **Healthy Reasoning Manifold** to a low-rank **Bias Manifold**. This confinement renders high-value solutions in the **Null Space** geometrically inaccessible, as the trajectory is trapped on a low-dimensional plane.

stagnates abruptly (Petrov et al., 2025). We argue that this is not merely a failure of generation, but a **geometric collapse of the representation space** (Li et al., 2025; Laurent et al., 2023; Fan et al., 2025).

Specifically, we posit the *Low-Rank Manifold Hypothesis*: as a strong model becomes overly confident in an erroneous reasoning path, its internal hidden states degenerate into a low-dimensional **Bias Manifold** (Minegishi et al., 2025; Bazarova et al., 2025; Phillips et al., 2025; Park et al., 2025). In this collapsed state, the model’s covariance matrix becomes ill-conditioned, as it retains high variance only in directions confirming its bias, while variance in corrective directions vanishes to zero (Dohmatob et al., 2024).

To transcend this geometric limitation, we introduce the concept of **Spectral Orthogonal Exploration (SOE)**. Our approach is grounded in a

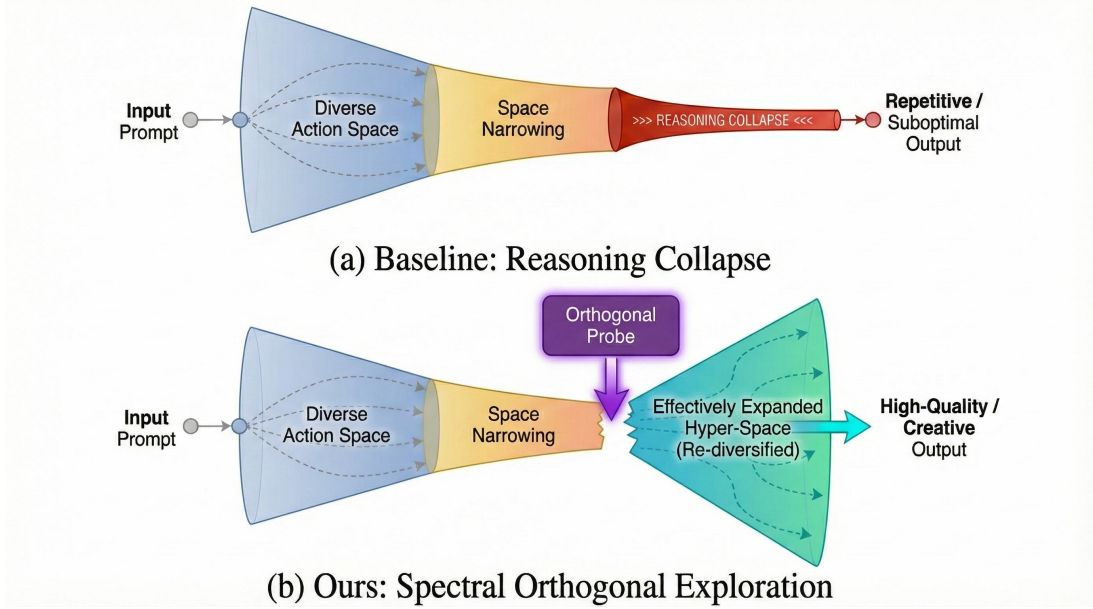


Figure 2: Mechanism of Spectral Orthogonal Exploration (SOE). To counteract space narrowing, we introduce an **Orthogonal Probe** as a geometric intervention. This force effectively disrupts the low-rank confinement and diversifies the reasoning trajectory, expanding the hyper-space to access high-quality solutions previously hidden in the teacher’s null space.

fundamental linear algebraic principle: escaping a restricted subspace necessitates a vector with a non-zero component in the subspace’s null space. We propose a counter-intuitive **Student Guides Teacher** paradigm, where a weaker Student model acts not as a supervisor, but as an **Orthogonal Probe**. Crucially, the Student’s utility derives not from its predictive accuracy, but from its structural heterogeneity. Since the Student has not converged toward the same Bias Manifold as the Teacher, its reasoning trajectories—though potentially suboptimal—often retain significant projections within the Teacher’s spectral blind spots. By calculating the **Orthogonal Projection Residual** of the Student’s outputs relative to the Teacher’s dominant eigenspace, we mathematically identify the **ejection force** required to liberate the Teacher from its cognitive fixation.

## 2 Related Work

Traditional alignment and exploration methods, such as high-temperature sampling (Holtzman et al., 2020) or diverse prompting, often struggle to rectify the structural pathology of reasoning collapse (Zhang et al., 2025; Lu et al., 2023; Gudibande et al., 2023; Casper et al., 2023; Ethayarajh, 2019; Shumailov et al., 2023). Because these methods operate primarily in the probabilistic token space, they implicitly assume that lexical

diversity equates to semantic exploration (Shi et al., 2025; Shypula et al., 2025).

However, from a geometric perspective, stochastic sampling on a collapsed manifold is similar to **Brownian motion restricted to a 2D plane**: no matter how much noise is injected, the trajectory cannot escape to the third dimension (Seddik et al., 2024; Joseph et al., 2025; Farghly et al., 2025). Consequently, the model generates fluent and diverse yet logically redundant fallacies, remaining effectively trapped within a spectral “blind spot” that stochasticity alone cannot illuminate.

## 3 Motivation: The Geometry of Reasoning Collapse

To understand the nature of reasoning failure, we move beyond surface-level token statistics to analyze the geometric properties of the model’s representation space. While reasoning collapse is often identified by repetitive text or logical loops, we posit that these are merely linguistic manifestations of a deeper geometric pathology known as **Spectral Collapse**.

### 3.1 The Low-Rank Manifold Hypothesis

Consider the inference process of a Large Language Model as a discrete dynamical system. We define the hidden state trajectory of a reasoning chain up to step  $t$  as  $H_t = [h_1, h_2, \dots, h_t] \in \mathbb{R}^{t \times d}$ ,

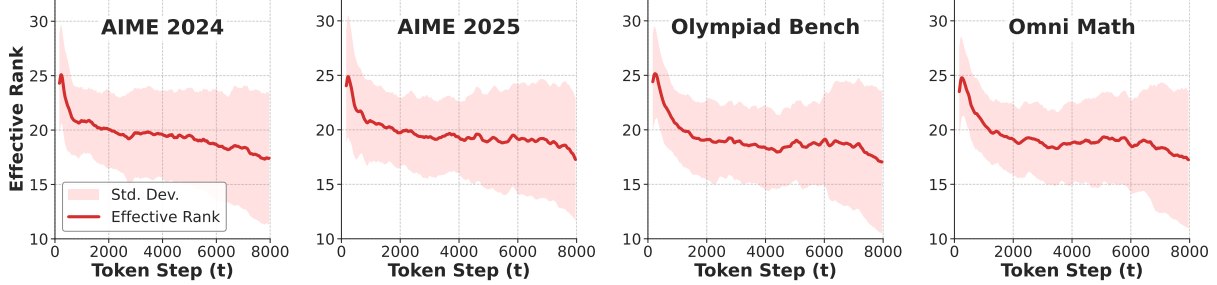


Figure 3: **Universality of Reasoning Collapse across Datasets.** The dynamics of Effective Rank during the reasoning process on AIME 24, AIME 25, Olympiad Bench and Omni Math. Across all benchmarks, we observe a consistent spectral degeneration pattern: as the token steps increase, the effective rank of the covariance matrix decays, indicating the model is collapsing into a low-dimensional bias manifold regardless of the problem difficulty.

formed by stacking the hidden state vectors. Specifically, the  $i$ -th row represents the hidden state  $h_i \in \mathbb{R}^{1 \times d}$  at step  $i$ . As the model commits to a specific reasoning path, its internal representations tend to congregate within a lower-dimensional subspace. To describe the dimension of the subspace, we analyze the *Local Covariance Matrix*  $\Sigma_t$  of the recent window of  $k$  tokens:

$$\Sigma_t = \frac{1}{k-1} \sum_{i=t-k+1}^t (h_i - \mu_t)^\top (h_i - \mu_t) \quad (1)$$

where  $\mu_t$  is the local mean. If the dimension of subspace is low, the hidden state will be more similar, then the *Local Covariance Matrix* would have a lower rank. Based on this, we posit the **Low-Rank Manifold Hypothesis**: during reasoning collapse, the rank of  $\Sigma_t$  will decrease, confining the reasoning process to a **Bias Manifold**  $\mathcal{M}$  (Gao et al., 2019).

### 3.2 Quantifying Spectral Collapse

Based on previous analysis, to measure the dimensionality of this bias manifold, we need to calculate the rank of  $\Sigma_t$ . We employ the Effective Rank (*EffRank*) (Roy and Vetterli, 2007) to achieve our goal, which measures the effective information content of the spectrum:

$$EffRank(\Sigma_t) = \exp \left( - \sum_{j=1}^d \tilde{\sigma}_j \log \tilde{\sigma}_j \right) \quad (2)$$

Here,  $\tilde{\sigma}_j = \lambda_j / \sum_{i=1}^d \lambda_i$  represents the normalized singular values. A mathematical collapse is characterized by  $EffRank(\Sigma_t) \ll d$ . In this state, the variance in directions orthogonal to the null space  $\mathcal{M}$  vanishes to zero. Consequently, even with stochastic sampling (temperature  $T > 0$ ), the

generated tokens were trapped in the Bias Manifold, rendering the model blind to correct solutions that lie in the null space.

### 3.3 Empirical Analysis

To verify our hypothesis, we conducted pilot experiment across four challenging mathematical benchmarks: AIME 24 (Patel et al., 2024), AIME 25 (Petrov et al., 2025), OlympiadBench (He et al., 2024) and OmniMath (Gao et al., 2024). We choose Qwen3-4B-Instruct-2507 (Team, 2025b) to sample reasoning chains with a high temperature ( $T = 0.7$ ). To specifically isolate the phenomenon of reasoning collapse, we curate a dataset by filtering for trajectories that are both factually incorrect and exhibit excessive verbosity (exceeding 4,000 tokens). For each selected trajectory, we computed the Effective Rank of the covariance matrix of the final hidden states using a sliding window of size  $k = 64$ .

As illustrated in Figure 3, we observe a significant decrease of numerical rank of the representation space in long, erroneous reasoning chains. Despite a theoretical full rank of  $d = 2560$ , the effective dimensionality consistently decays as the generation progresses. This quantitative evidence validates our hypothesis that reasoning loops stem from a physical collapse into a low-dimensional bias manifold, where the model is deprived of the geometric degrees of freedom essential for divergent exploration. Such a structural limitation necessitates a geometric intervention to actively expand the exploration space.

To further substantiate the universality of these findings, we provide an extended analysis in Appendix B. There, we demonstrate that reasoning collapse is a model-agnostic phenomenon observable across various model sizes.

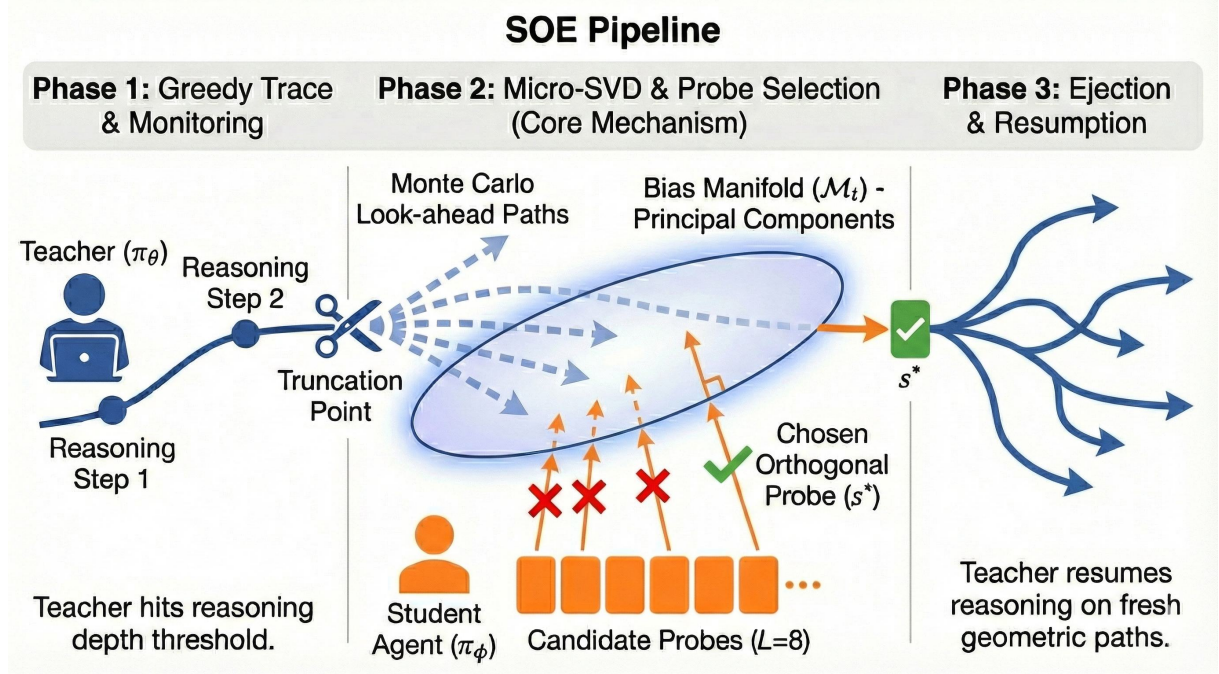


Figure 4: The SOE Framework

## 4 Methodology: The SOE Framework

Motivated by the observed geometric decay, we develop the **Spectral Orthogonal Exploration (SOE)** framework. This section details the SOE algorithm designed to detect reasoning collapse and strategically intervene reasoning collapse during the inference process.

### 4.1 Overview of the Geometric Interaction

The framework operates on a post-hoc intervention paradigm. As shown in Figure 4, the process follows three stages:

- Greedy Trace and Monitoring:** We first employ the Teacher  $\pi_\theta$  to generate a complete reasoning chain via greedy decoding. We then collect trajectories that yield incorrect answers, treating these erroneous paths as the baseline for collapsed reasoning. These trajectories are then partitioned at critical reasoning milestones (e.g., the onset of logical steps). This procedure yields a set of prefix trajectories, allowing us to probe the model's latent state at various depths of the reasoning process.
- Micro-SVD and Probe Selection:** At each truncation point  $t_i$ , we estimate the local bias manifold  $\mathcal{M}_t$  using Monte Carlo look-ahead simulations and Micro-SVD to identify the

subspace where the Teacher model is trapped. For each truncation point, the Student  $\pi_\phi$  generates candidate "probe" sequences (fixed at  $L = 8$  tokens). We calculate the orthogonality of these candidates relative to the specific manifold  $\mathcal{M}_t$  at that step, selecting the optimal probe  $s_t^*$  that maximizes the orthogonality score.

- Ejection and Resumption:** The previous process yields distinct intervened contexts (the truncated histories stitched with their respective orthogonal probes). The Teacher  $\pi_\theta$  then resumes reasoning via sampling from each of these modified contexts, effectively attempting to recover the correct solution from three different geometric "ejection points".

A detailed example of the algorithm is provided in Appendix A.

### 4.2 Manifold Estimation

To estimate the bias manifold of the Teacher, we assume the Teacher's internal representations at truncation point  $t$  follow a local distribution with covariance  $\Sigma_t$ . Our goal is to obtain an *unbiased estimate* of the principal components of  $\Sigma_t$ .

**Unbiased Covariance Estimator.** Given the context  $x_{$

$\pi_\theta(\cdot|x_{<t})$ . Let  $\mathbf{h}_i \in \mathbb{R}^d$  be the aggregated hidden state of the  $i$ -th trajectory. We calculate the sample mean  $\hat{\mu} = \frac{1}{N} \sum_{i=1}^N \mathbf{h}_i$  and construct the centered state matrix  $\mathbf{H} \in \mathbb{R}^{d \times N}$ :

$$\mathbf{H} = [\mathbf{h}_1 - \hat{\mu}, \dots, \mathbf{h}_N - \hat{\mu}] \quad (3)$$

Theoretically, the sample covariance matrix  $\hat{\mathbf{C}} = \frac{1}{N-1} \mathbf{H} \mathbf{H}^T$  serves as an unbiased estimator of the true population covariance  $\Sigma_t$ . By analyzing the spectrum of  $\hat{\mathbf{C}}$ , we can recover the directions of maximum variance that the model is naturally collapsing into.

**The Micro-SVD Algorithm.** Directly computing eigenvectors for  $\hat{\mathbf{C}} \in \mathbb{R}^{d \times d}$  is computationally prohibitive. We leverage the SVD duality, computing the Gram Matrix  $\mathbf{G} \in \mathbb{R}^{N \times N}$  of our Monte Carlo samples:

$$\mathbf{G} = \mathbf{H}^T \mathbf{H} \quad (4)$$

Solving the eigen-problem for the smaller matrix  $\mathbf{G} \mathbf{v}_k = \lambda_k \mathbf{v}_k$  allows us to recover the principal components  $\mathbf{u}_k$  of the Teacher’s manifold:

$$\mathbf{u}_k = \frac{1}{\sqrt{\lambda_k}} \mathbf{H} \mathbf{v}_k \quad (5)$$

We define the **Bias Manifold**  $\mathcal{M}_t$  as the subspace spanned by the top- $k$  eigenvectors  $\mathbf{U}_\parallel = \{\mathbf{u}_1, \dots, \mathbf{u}_k\}$ . Directions orthogonal to this space constitute the "Null Space" where potential creative solutions reside.

### 4.3 Probe Selection: Orthogonal Latent Stitching (OLS)

With the manifold  $\mathcal{M}_t$  identified, we employ Orthogonal Latent Stitching to mechanically eject the model from its local optimum.

**Heterogeneous Probing.** The Student model  $\pi_\phi$  generates a set of candidate sequences  $\mathcal{C}_{Student} = \{s_1, \dots, s_M\}$ , each with a fixed length of  $L = 8$  tokens. These short sequences act as geometric impulse vectors. To evaluate their geometry, we map them into the Teacher’s latent space via a forward pass:  $\mathbf{z}_j = \text{Forward}_{\pi_\theta}(s_j|x_{<t})$ .

**Residual Maximization.** We compute the projection of each candidate  $\mathbf{z}_j$  onto the Teacher’s bias manifold using the projection operator  $\mathbf{P}_\parallel = \mathbf{U}_\parallel \mathbf{U}_\parallel^T$ . The orthogonal residual  $\mathbf{r}_j$  represents the component of the Student’s thought that lies strictly in the Teacher’s blind spot:

$$\mathbf{r}_j = (\mathbf{I} - \mathbf{P}_\parallel)(\mathbf{z}_j - \hat{\mu}) \quad (6)$$

We select the candidate  $s^*$  that maximizes the Orthogonality Score, defined as the normalized energy of this residual, where  $\epsilon > 0$  is a small constant introduced to avoid division by zero:

$$s^* = \arg \max_{s_j \in \mathcal{C}_{Student}} \frac{\|\mathbf{r}_j\|_2}{\|\mathbf{z}_j - \hat{\mu}\|_2 + \epsilon} \quad (7)$$

This orthogonal token sequence  $s^*$  is stitched to the truncated context, forcing the Teacher to resolve the reasoning path from a new geometric coordinate outside its original bias manifold.

## 5 Experiments

To validate the theoretical claims of Spectral Orthogonal Exploration (SOE), we conducted extensive experiments focused on high-difficulty mathematical reasoning tasks.

### 5.1 Experimental Setup

**Models.** We adopt a “Weak-Student and Strong-Teacher” configuration to validate our proposal: We use Qwen3-4B-Instruct-2507 as the Teacher, and use Gemma-3-4B-IT (Team, 2025a) as the Student. Crucially, the Student’s different architecture and training data ensures that its bias manifold is not perfectly aligned with the Teacher’s.

**Datasets.** We evaluate performance on five challenging mathematical benchmarks: AIME 2024, AIME 2025, MATH-500 (Hendrycks et al., 2021), OlympiadBench and Omni-Math. Given the strong capabilities of the Teacher model, we specifically selected problems from Omni-Math with a difficulty level greater than or equal to 8.

Dataset	Teacher	Student
AIME 2024	<b>50.0%</b>	13.3%
AIME 2025	<b>33.7%</b>	6.7%
MATH-500	<b>86.8%</b>	71.2%
Olympiad Bench	<b>45.3%</b>	27.7%
Omni-Math(Hard)	<b>18.3%</b>	4.2%

Table 2: Comparison of fundamental capabilities between Teacher and Student models on mathematical benchmarks. Both the Teacher and Student are evaluated under identical conditions, with same prompt, greedy decoding and a maximum context length capped at 8192 tokens.

**Evaluation** For all benchmarks, model outputs are post-processed using a combination of

Method	AIME 24	AIME 25	MATH-500	Olympiad	Omni-Math (Hard)	Average
Baseline (Self-Consistency)	38.5%	35.3%	33.7%	11.7%	14.5%	26.7%
<b>Ours (SOE)</b>	<b>76.9%</b>	<b>70.6%</b>	<b>45.9%</b>	<b>15.5%</b>	<b>20.8%</b>	<b>45.9%</b>
Relative Improvement	+99.7%	+100.0%	+36.2%	+32.5%	+43.4%	+62.4%

Table 1: Pass@16 accuracy on the **Difficult Subset** (problems where Teacher’s greedy decoding failed). SOE demonstrates a consistent improvement over the Baseline, confirming that directed orthogonal exploration is superior to random perturbation. All the results are sampled under identical conditions, with same prompt, *temperature* = 0.7 and a maximum context (sampling) length capped at 8192 tokens.

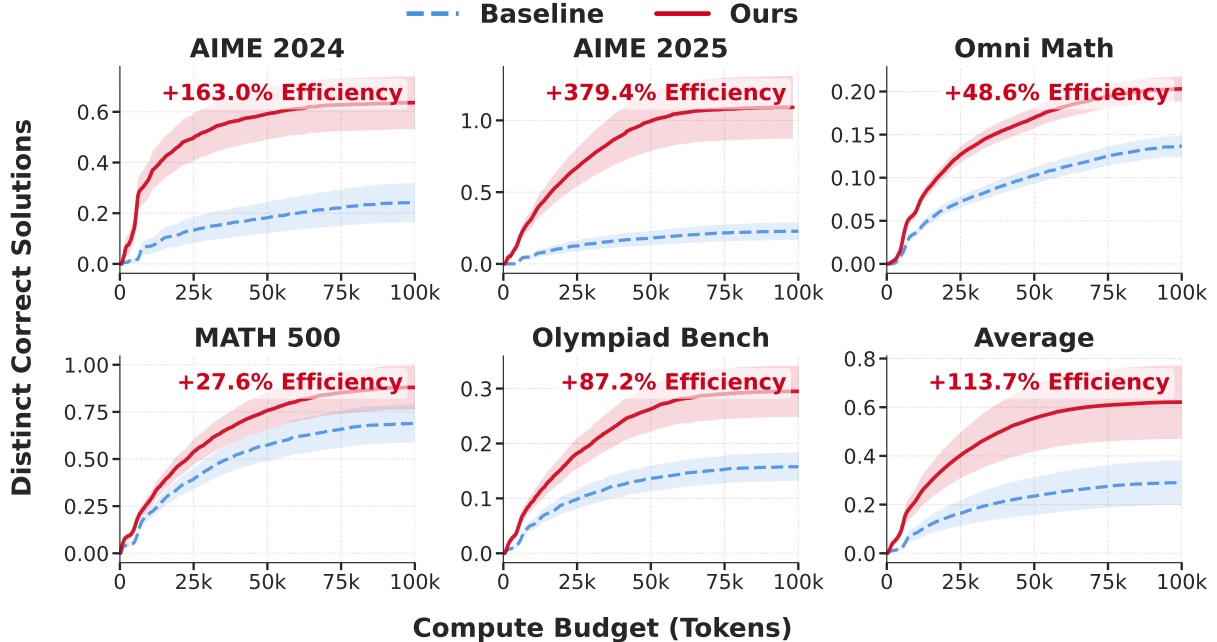


Figure 5: Semantic Exploration Efficiency. The curves depict the cumulative number of distinct correct solutions discovered as a function of the compute budget (total tokens). SOE significantly outperforms the Baseline by maintaining a near-linear discovery rate, whereas the Baseline exhibits logarithmic saturation.

regular-expression-based normalization and the MathEvaluator library to extract and verify final answers against ground truth.

**Baselines and Implementation Details.** We compare three experimental settings:

- **Baseline (Self-Consistency):** Standard sampling with the Teacher model ( $T = 0.7$ ). This represents the control group for stochastic exploration within the Bias Manifold.
- **Ours (SOE):** We generate  $N = 8$  candidates from the Student ( $T = 1.0$ ), compute their embeddings using the Teacher model, and mechanically stitch the candidate maximizing the Orthogonality Score ( $\Omega(s) \rightarrow 1$ ) into the Teacher’s context. The subsequent reasoning chain is completed by the Teacher ( $T = 0.7$ ).

## 5.2 Main Results

We evaluate the solution accuracy using **Pass@16**. As shown in Table 1, SOE significantly outperforms the Baseline methods across all datasets on the difficult subset.

## 5.3 Exploration Efficiency

Given the proposed Spectral Orthogonal Exploration (SOE) introduces additional inference costs, it is important to assess its cost-effectiveness relative to standard sampling methods. To this end, we evaluate the **Semantic Exploration Efficiency** of our approach compared to the Self-Consistency baseline. We measure the relationship between the computational budget (quantified by the total number of tokens generated) and the discovery rate of *semantically distinct* correct reasoning trajectories.

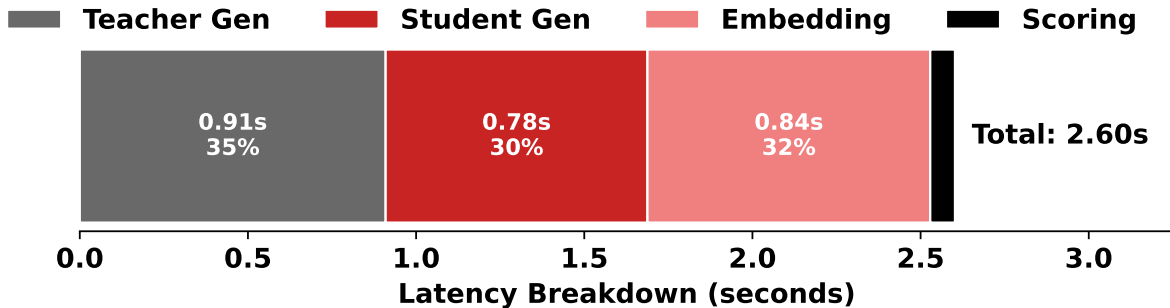


Figure 6: Latency breakdown of a single SOE intervention step evaluated on the AIME 2025 benchmark. The process was measured on an NVIDIA A800 GPU using the standard Hugging Face generation pipeline.

**Metric Definition.** We used jina (Günther et al., 2023) to compute embeddings for all generated correct solution traces. A solution is considered “new” only if its cosine similarity with all previously found correct solutions is below a threshold of  $\tau = 0.95$ . This filters out trivial rephrasings.

As illustrated in Figure 5, our method achieves significantly higher sampling efficiency than the baseline approach.

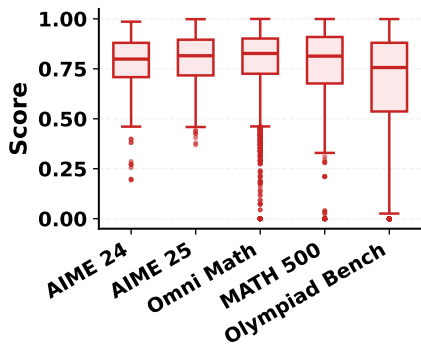


Figure 7: **Distribution of Orthogonality Scores** for Student-generated probes across benchmarks. The score ranges from 0 to 1, where a value of 1 indicates perfect orthogonality relative to the Teacher’s Bias Manifold, and 0 denotes complete alignment (collinearity).

To validate the geometric mechanism driving this efficiency, we further analyze the distribution of Orthogonality Scores in Figure 7. Across all benchmarks, the Student-generated probes consistently exhibit high orthogonality relative to the Teacher’s local Bias Manifold. This empirical evidence confirms that the Student’s outputs possess sufficient structural heterogeneity to project effectively onto the Teacher’s orthogonal space (Null Space), thereby serving as valid geometric interventions to escape low-rank confinement.

As detailed in Figure 6, measurements con-

ducted on the AIME 2025 benchmark using NVIDIA A800 GPUs reveal a total latency of approximately 2.60s per intervention step via the standard transformers.generate pipeline. We deem this trade-off acceptable given the substantial gain in discovering valid reasoning trajectories.

Due to space constraints, comprehensive ablation studies validating the contribution of each component and robustness experiments across different model scales are detailed in Appendix C.

## 6 Analysis: The Thermodynamics of Reasoning

Based on our analysis, we argue “Reasoning Collapse” is mathematically equivalent to the *Rank Collapse* of the hidden state covariance matrix.

In this section, we provide a theoretical justification for two phenomena: (1) Why LLMs naturally degenerate into low-rank manifolds, and (2) Why our Orthogonal Latent Stitching (OLS) acts as a geometric dimensional expander rather than a knowledge injector.

### 6.1 The Trap of Low-Rank Self-Consistency

Let  $H_t \in \mathbb{R}^{N \times d}$  be the matrix of hidden states in the context window at step  $t$ . We define the local covariance matrix  $\Sigma_t = \frac{1}{N-1} H_t^T H_t$ . Reasoning collapse occurs when the effective rank of  $\Sigma_t$  diminishes, i.e.,  $\text{rank}(\Sigma_t) \ll d$ . The states are confined to a subspace  $\mathcal{S}$ .

**Proposition 1 (Invariance of Subspace).** *If the input context lies within a low-rank subspace  $\mathcal{S}$ , the output of a standard Self-Attention layer lies strictly within the same subspace (or a linear transform thereof), preventing spontaneous exploration of the Null Space. (Dong et al., 2021; Wang et al., 2020)*

The detailed proof and an analysis of why non-linearities (FFNs) fail to restore dimensionality are provided in Appendix D.1.

## 6.2 Theoretical Justification for Progressive Rank Decay

Why does the effective rank decrease over time during long chain-of-thought reasoning? We attribute this to the **Spectrum Contraction** property of the Softmax operator in high-confidence regimes (Yang et al., 2017).

**Theorem 2 (Spectrum Contraction).** *As the model becomes more confident (the norm of logits increases), the attention mechanism acts as a rank-reducing operator, causing the spectrum of the covariance matrix to decay exponentially.*

Please refer to Appendix D.2 for the formal proof. Thus, reasoning behaves like a *contractive mapping* on the manifold dimension. The model "forgets" the orthogonal dimensions required for error correction.

## 6.3 Orthogonal Injection: Geometry vs. Information

A critical question arises: Does SOE work because the Student provides *new knowledge* (Information Injection), or because it *opens space* (Geometric Injection)? We prove it is the latter by analyzing the signal-to-noise ratio in the Null Space.

**Geometric Infinity (The "Dimension Attack").** Consider the contribution to the spectrum in the Null Space direction  $u_\perp$ . Prior to injection, the variance in this direction is  $\sigma_\perp^2 \approx 0$ . After injecting an orthogonal vector  $v_\perp$  (where  $\|v_\perp\| > 0$ ):

- Old Signal-to-Noise Ratio (SNR) in  $\mathcal{S}^\perp$ :  $0/\epsilon = 0$ .
- New Signal-to-Noise Ratio in  $\mathcal{S}^\perp$ :  $\|v_\perp\|^2/\epsilon \rightarrow \infty$ .

Even a semantically "weak" or "nonsense" token, if orthogonal, introduces a non-zero eigenvalue  $\lambda_{new} > 0$  to the covariance matrix (see Appendix D.3 for the Semantic Sparsity analysis).

$$\text{rank}(\Sigma_{new}) = \text{rank}(\Sigma_{old}) + 1 \quad (8)$$

This topological change (increasing the rank) is discontinuous and drastic. It creates a new dimension for the inference trajectory to evolve, effectively converting a local minimum (saddle point in flat space) into a slope. Therefore, SOE functions

primarily as a **Dimensionality Expander**, creating a "wormhole" out of the low-rank Bias Manifold.

## 7 Conclusion

We attribute *Reasoning Collapse* to a geometric degeneration into low-rank *Bias Manifold*, rendering high-value solutions in the *Null Space* inaccessible. To address this, we introduce **Spectral Orthogonal Exploration (SOE)**, which employs a "Student Guides Teacher" paradigm to mechanically eject models from local optima via *Orthogonal Latent Stitching*. Our analysis confirms that SOE functions fundamentally as a *Dimensionality Expander* rather than a knowledge injector. These findings suggest that overcoming reasoning bottlenecks requires moving beyond probabilistic sampling toward precise geometric interventions in the latent space.

## 8 Limitations

While our proposed Spectral Orthogonal Exploration (SOE) framework demonstrates significant efficacy in mitigating reasoning collapse, we acknowledge several limitations that merit further investigation.

First, regarding computational efficiency, although SOE improves sample efficiency by requiring fewer total tokens to discover correct solutions, it introduces additional wall-clock latency per reasoning step. This is due to the computational overhead of the Micro-SVD operation and Monte Carlo look-ahead simulations required to estimate the Bias Manifold  $\mathcal{M}_t$ .

Second, the core mechanism of SOE relies on explicitly accessing and manipulating the model's internal hidden states to compute effective rank and orthogonal residuals. This requirement restricts the applicability of our method to open-weights models, precluding its direct use with closed-source LLMs where only API access is available.

Finally, due to computational resource constraints, our empirical validation is primarily conducted on models in the 4B parameter range within mathematical domains. While our theoretical analysis suggests the Low-Rank Manifold Hypothesis is model-agnostic, further research is needed to verify the scalability of SOE on substantially larger models and its generalization to other reasoning-intensive tasks beyond mathematics.

## References

Alexandra Bazarova, Aleksandr Yugay, Andrey Shulga, Alina Ermilova, Andrei Volodichev, Konstantin Polev, Julia Belikova, Rauf Parchiev, Dmitry Simakov, Maxim Savchenko, Andrey Savchenko, Serguei Barannikov, and Alexey Zaytsev. 2025. Hallucination detection in llms with topological divergence on attention graphs. *Preprint*, arXiv:2504.10063.

Sébastien Bubeck, Christian Coester, Ronen Eldan, Timothy Gowers, Yin Tat Lee, Alexandru Lupsasca, Mehtaab Sawhney, Robert Scherrer, Mark Sellke, Brian K. Spears, Derya Unutmaz, Kevin Weil, Steven Yin, and Nikita Zhivotovskiy. 2025. Early science acceleration experiments with gpt-5. *Preprint*, arXiv:2511.16072.

Stephen Casper, Xander Davies, Claudia Shi, Thomas Krendl Gilbert, Jérémie Scheurer, Javier Rando, Rachel Freedman, Tomasz Korbak, David Lindner, Pedro Freire, and 1 others. 2023. Open problems and fundamental limitations of reinforcement learning from human feedback. *arXiv preprint arXiv:2307.15217*.

DeepSeek-AI, Daya Guo, Dejian Yang, Haowei Zhang, Junxiao Song, Ruoyu Zhang, Runxin Xu, Qihao Zhu, Shirong Ma, Peiyi Wang, Xiao Bi, Xiaokang Zhang, Xingkai Yu, Yu Wu, Z. F. Wu, Zhibin Gou, Zhi-hong Shao, Zhuoshu Li, Ziyi Gao, and 181 others. 2025a. Deepseek-r1: Incentivizing reasoning capability in llms via reinforcement learning. *Preprint*, arXiv:2501.12948.

DeepSeek-AI, Aixin Liu, Bei Feng, Bing Xue, Bingxuan Wang, Bochao Wu, Chengda Lu, Chenggang Zhao, Chengqi Deng, Chenyu Zhang, Chong Ruan, Damai Dai, Daya Guo, Dejian Yang, Deli Chen, Dongjie Ji, Erhang Li, Fangyun Lin, Fucong Dai, and 181 others. 2025b. Deepseek-v3 technical report. *Preprint*, arXiv:2412.19437.

DeepSeek-AI, Aixin Liu, Aoxue Mei, Bangcai Lin, Bing Xue, Bingxuan Wang, Bingzheng Xu, Bochao Wu, Bowei Zhang, Chaofan Lin, Chen Dong, Chengda Lu, Chenggang Zhao, Chengqi Deng, Chen-hao Xu, Chong Ruan, Damai Dai, Daya Guo, Dejian Yang, and 245 others. 2025c. Deepseek-v3.2: Pushing the frontier of open large language models. *Preprint*, arXiv:2512.02556.

Elvis Dohmatob, Yunzhen Feng, and Julia Kempe. 2024. Model collapse demystified: The case of regression. *Preprint*, arXiv:2402.07712.

Yihe Dong, Jean-Baptiste Cordonnier, and Andreas Loukas. 2021. Attention is not all you need: Pure attention loses rank doubly exponentially with depth. In *International conference on machine learning*, pages 2793–2803. PMLR.

Kawin Ethayarajh. 2019. How contextual are contextualized word representations? comparing the geometry of bert, elmo, and gpt-2 embeddings. *arXiv preprint arXiv:1909.00512*.

Ziqing Fan, Siyuan Du, Shengchao Hu, Pingjie Wang, Li Shen, Ya Zhang, Dacheng Tao, and Yanfeng Wang. 2025. Combatting dimensional collapse in llm pre-training data via diversified file selection. *Preprint*, arXiv:2504.20644.

Tyler Farghly, Peter Potapchik, Samuel Howard, George Deligiannidis, and Jakiw Pidstrigach. 2025. Diffusion models and the manifold hypothesis: Log-domain smoothing is geometry adaptive. *Preprint*, arXiv:2510.02305.

Bofei Gao, Feifan Song, Zhe Yang, Zefan Cai, Yibo Miao, Qingxiu Dong, Lei Li, Chenghao Ma, Liang Chen, Runxin Xu, Zhengyang Tang, Benyou Wang, Daoguang Zan, Shanghaoran Quan, Ge Zhang, Lei Sha, Yichang Zhang, Xuancheng Ren, Tianyu Liu, and Baobao Chang. 2024. Omni-math: A universal olympiad level mathematic benchmark for large language models. *Preprint*, arXiv:2410.07985.

Jun Gao, Di He, Xu Tan, Tao Qin, Liwei Wang, and Tie-Yan Liu. 2019. Representation degeneration problem in training natural language generation models. *arXiv preprint arXiv:1907.12009*.

Mor Geva, Roei Schuster, Jonathan Berant, and Omer Levy. 2021. Transformer feed-forward layers are key-value memories. In *Proceedings of the 2021 Conference on Empirical Methods in Natural Language Processing*, pages 5484–5495.

Arnav Gudibande, Eric Wallace, Charlie Snell, Xinyang Geng, Hao Liu, Pieter Abbeel, Sergey Levine, and Dawn Song. 2023. The false promise of imitating proprietary llms. *arXiv preprint arXiv:2305.15717*.

Dadi Guo, Jiayu Liu, Zhiyuan Fan, Zhitao He, Haoran Li, Yuxin Li, Yumeng Wang, and Yi R. Fung. 2025. Mathematical proof as a litmus test: Revealing failure modes of advanced large reasoning models. *Preprint*, arXiv:2506.17114.

Michael Günther, Jackmin Ong, Isabelle Mohr, Alaeddine Abdessalem, Tanguy Abel, Mohammad Kalim Akram, Susana Guzman, Georgios Mastrapas, Saba Sturua, Bo Wang, Maximilian Werk, Nan Wang, and Han Xiao. 2023. Jina embeddings 2: 8192-token general-purpose text embeddings for long documents. *Preprint*, arXiv:2310.19923.

Chaoqun He, Renjie Luo, Yuzhuo Bai, Shengding Hu, Zhen Thai, Junhao Shen, Jinyi Hu, Xu Han, Yujie Huang, Yuxiang Zhang, and 1 others. 2024. Olympiadbench: A challenging benchmark for promoting agi with olympiad-level bilingual multimodal scientific problems. In *Proceedings of the 62nd Annual Meeting of the Association for Computational Linguistics (Volume 1: Long Papers)*, pages 3828–3850.

Dan Hendrycks, Collin Burns, Saurav Kadavath, Akul Arora, Steven Basart, Eric Tang, Dawn Song, and Jacob Steinhardt. 2021. Measuring mathematical problem solving with the math dataset. *arXiv preprint arXiv:2103.03874*.

Jordan Hoffmann, Sebastian Borgeaud, Arthur Mensch, Elena Buchatskaya, Trevor Cai, Eliza Rutherford, Diego de Las Casas, Lisa Anne Hendricks, Johannes Welbl, Aidan Clark, Tom Hennigan, Eric Noland, Katie Millican, George van den Driessche, Bogdan Damoc, Aurelia Guy, Simon Osindero, Karen Simonyan, Erich Elsen, and 3 others. 2022. [Training compute-optimal large language models](#). *Preprint*, arXiv:2203.15556.

Ari Holtzman, Jan Buys, Li Du, Maxwell Forbes, and Yejin Choi. 2020. [The curious case of neural text degeneration](#). *Preprint*, arXiv:1904.09751.

Federico Arangath Joseph, Jerome Sieber, Melanie N. Zeilinger, and Carmen Amo Alonso. 2025. [Lambda-skip connections: the architectural component that prevents rank collapse](#). *Preprint*, arXiv:2410.10609.

Jared Kaplan, Sam McCandlish, Tom Henighan, Tom B Brown, Benjamin Chess, Rewon Child, Scott Gray, Alec Radford, Jeffrey Wu, and Dario Amodei. 2020. [Scaling laws for neural language models](#). *arXiv preprint arXiv:2001.08361*.

Thomas Laurent, James H. von Brecht, and Xavier Bresson. 2023. [Feature collapse](#). *Preprint*, arXiv:2305.16162.

Melody Zixuan Li, Kumar Krishna Agrawal, Arna Ghosh, Komal Kumar Teru, Adam Santoro, Guil-Jaume Lajoie, and Blake A. Richards. 2025. [Tracing the representation geometry of language models from pretraining to post-training](#). *Preprint*, arXiv:2509.23024.

Pan Lu, Liang Qiu, Wenhao Yu, Sean Welleck, and Kai-Wei Chang. 2023. [A survey of deep learning for mathematical reasoning](#). In *Proceedings of the 61st annual meeting of the association for computational linguistics (volume 1: long papers)*, pages 14605–14631.

Gouki Minegishi, Hiroki Furuta, Takeshi Kojima, Yusuke Iwasawa, and Yutaka Matsuo. 2025. [Topology of reasoning: Understanding large reasoning models through reasoning graph properties](#). *Preprint*, arXiv:2506.05744.

Seongheon Park, Xuefeng Du, Min-Hsuan Yeh, Haobo Wang, and Yixuan Li. 2025. [Steer llm latents for hallucination detection](#). *Preprint*, arXiv:2503.01917.

Bhrij Patel, Souradip Chakraborty, Wesley A. Suttle, Mengdi Wang, Amrit Singh Bedi, and Dinesh Manocha. 2024. [Aime: Ai system optimization via multiple llm evaluators](#). *Preprint*, arXiv:2410.03131.

Ivo Petrov, Jasper Dekoninck, Lyuben Baltadzhiev, Maria Drencheva, Kristian Minchev, Mislav Balunović, Nikola Jovanović, and Martin Vechev. 2025. [Proof or bluff? evaluating llms on 2025 usa math olympiad](#). *Preprint*, arXiv:2503.21934.

Edward Phillips, Sean Wu, Soheila Molaei, Danielle Belgrave, Anshul Thakur, and David Clifton. 2025. [Geometric uncertainty for detecting and correcting hallucinations in llms](#). *Preprint*, arXiv:2509.13813.

Olivier Roy and Martin Vetterli. 2007. [The effective rank: A measure of effective dimensionality](#). In *2007 15th European signal processing conference*, pages 606–610. IEEE.

Mohamed El Amine Seddik, Suei-Wen Chen, Soufiane Hayou, Pierre Youssef, and Merouane Debbah. 2024. [How bad is training on synthetic data? a statistical analysis of language model collapse](#). *Preprint*, arXiv:2404.05090.

Weijie Shi, Yue Cui, Yaguang Wu, Jingzhi Fang, Shibo Zhang, Mengze Li, Sirui Han, Jia Zhu, Jiajie Xu, and Xiaofang Zhou. 2025. [Semantic-guided diverse decoding for large language model](#). *Preprint*, arXiv:2506.23601.

Parshin Shojaee, Iman Mirzadeh, Keivan Alizadeh, Maxwell Horton, Samy Bengio, and Mehrdad Farajtabar. 2025. [The illusion of thinking: Understanding the strengths and limitations of reasoning models via the lens of problem complexity](#). *Preprint*, arXiv:2506.06941.

Ilia Shumailov, Zakhar Shumaylov, Yiren Zhao, Yarin Gal, Nicolas Papernot, and Ross Anderson. 2023. [The curse of recursion: Training on generated data makes models forget](#). *arXiv preprint arXiv:2305.17493*.

Alexander Shypula, Shuo Li, Botong Zhang, Vishakh Padmakumar, Kayo Yin, and Osbert Bastani. 2025. [Evaluating the diversity and quality of llm generated content](#). *Preprint*, arXiv:2504.12522.

Gemma Team. 2025a. [Gemma 3](#).

Qwen Team. 2025b. [Qwen3 technical report](#). *Preprint*, arXiv:2505.09388.

Qwen Team. 2025c. [Qwq-32b: Embracing the power of reinforcement learning](#).

Sinong Wang, Belinda Z Li, Madian Khabsa, Han Fang, and Hao Ma. 2020. [Linformer: Self-attention with linear complexity](#). *arXiv preprint arXiv:2006.04768*.

Jason Wei, Yi Tay, Rishi Bommasani, Colin Raffel, Barret Zoph, Sebastian Borgeaud, Dani Yogatama, Maarten Bosma, Denny Zhou, Donald Metzler, Ed H. Chi, Tatsunori Hashimoto, Oriol Vinyals, Percy Liang, Jeff Dean, and William Fedus. 2022. [Emergent abilities of large language models](#). *Preprint*, arXiv:2206.07682.

Khurram Yamin, Shantanu Gupta, Gaurav R. Ghosal, Zachary C. Lipton, and Bryan Wilder. 2025. [Failure modes of llms for causal reasoning on narratives](#). *Preprint*, arXiv:2410.23884.

Zhilin Yang, Zihang Dai, Ruslan Salakhutdinov, and William W Cohen. 2017. Breaking the softmax bottleneck: A high-rank rnn language model. *arXiv preprint arXiv:1711.03953*.

Yue Zhang, Yafu Li, Leyang Cui, Deng Cai, Lemao Liu, Tingchen Fu, Xinting Huang, Enbo Zhao, Yu Zhang, Yulong Chen, and 1 others. 2025. Siren’s song in the ai ocean: A survey on hallucination in large language models. *Computational Linguistics*, pages 1–46.

Chengshuai Zhao, Zhen Tan, Pingchuan Ma, Dawei Li, Bohan Jiang, Yancheng Wang, Yingzhen Yang, and Huan Liu. 2025. [Is chain-of-thought reasoning of llms a mirage? a data distribution lens](#). *Preprint*, arXiv:2508.01191.

## A Detailed Example of Spectral Orthogonal Exploration

In this section, we provide a step-by-step walk-through of the SOE pipeline on a specific problem from the AIME 2025 dataset. We visualize the breakdown of the Teacher’s reasoning collapse and how the Student’s orthogonal probe successfully ejects the generation from the Bias Manifold.

### A.1 Problem Input

**Input Prompt**

**System Prompt:** Please reason step by step, and put your final answer within `\boxed{}`.

**User Problem:** In triangle  $ABC$  points  $D$  and  $E$  lie on  $\overline{AB}$  so that  $AD < AE < AB$ , while points  $F$  and  $G$  lie on  $\overline{AC}$  so that  $AF < AG < AC$ . Suppose  $AD = 4$ ,  $DE = 16$ ,  $EB = 8$ ,  $AF = 13$ ,  $FG = 52$ , and  $GC = 26$ . Let  $M$  be the reflection of  $D$  through  $F$ , and let  $N$  be the reflection of  $G$  through  $E$ . The area of quadrilateral  $DEGF$  is 288. Find the area of heptagon  $AFNBCM$ .

### A.2 Baseline: Reasoning Collapse (Greedy Decoding)

The Teacher model ( $\pi_\theta$ ) initially fails to solve the problem. Following is the generation.

We are given:

- Points  $D, E$  on  $AB$  such that  $AD < AE < AB$ ,
- Points  $F, G$  on  $AC$  such that  $AF < AG < AC$ ,
- Lengths:

- $AD = 4$
- $DE = 16$
- $EB = 8$
- $AF = 13$
- $FG = 52$
- $GC = 26$

- $M$  is the reflection of  $D$  through  $F$ ,
- $N$  is the reflection of  $G$  through  $E$ ,
- The area of quadrilateral  $DEGF$  is 288,
- Find the area of the heptagon  $AFNBCM$ .

### Step 1: Understand the given structure

**On segment  $AB$ :**

$$AD = 4, \quad DE = 16, \quad EB = 8$$

$$AB = AD + DE + EB = 4 + 16 + 8 = 30$$

**On segment  $AC$ :**

$$AF = 13, \quad FG = 52, \quad GC = 26$$

$$AC = AF + FG + GC = 13 + 52 + 26 = 91$$

### Step 2: Understanding points $M$ and $N$

- $M$  is the reflection of  $D$  through point  $F$ , meaning  $F$  is the midpoint of segment  $DM$ .
- $N$  is the reflection of  $G$  through point  $E$ , meaning  $E$  is the midpoint of segment  $GN$ .

Since  $D$  lies on  $AB$  while  $F$  lies on  $AC$ , the reflection is a point reflection in the plane, not along a line. Similarly,  $N$  need not lie on any side of triangle  $ABC$ .

The vertices of the required heptagon are

$$A, F, N, B, C, E, M.$$

### Step 3: Strategy

We aim to express the area of the heptagon  $AFNBCM$  in terms of the area of triangle  $ABC$ . However, since points  $M$  and  $N$  lie outside triangle  $ABC$ , the heptagon extends beyond the triangle, and we cannot simply subtract interior regions.

Thus, we adopt a vector-area approach.

#### Step 4: Vector setup

Let

$$\vec{AB} = \vec{b}, \quad \vec{AC} = \vec{c}.$$

Then:

$$|\vec{b} \times \vec{c}| = AB \cdot AC \cdot \sin \theta = 30 \cdot 91 \cdot \sin \theta = 2730 \sin \theta.$$

Points along  $AB$ :

$$\vec{D} = \frac{4}{30} \vec{b} = \frac{2}{15} \vec{b}, \quad \vec{E} = \frac{20}{30} \vec{b} = \frac{2}{3} \vec{b}.$$

Points along  $AC$ :

$$\vec{F} = \frac{13}{91} \vec{c} = \frac{1}{7} \vec{c}, \quad \vec{G} = \frac{65}{91} \vec{c} = \frac{5}{7} \vec{c}.$$

#### Step 5: Area of quadrilateral $DEGF$

Using the polygon area formula,

$$[DEGF] = \frac{1}{2} \left| \vec{D} \times \vec{E} + \vec{E} \times \vec{G} + \vec{G} \times \vec{F} + \vec{F} \times \vec{D} \right|.$$

Compute each term:

$$\vec{D} \times \vec{E} = 0, \quad \vec{G} \times \vec{F} = 0,$$

$$\vec{E} \times \vec{G} = \frac{10}{21} (\vec{b} \times \vec{c}), \quad \vec{F} \times \vec{D} = -\frac{2}{105} (\vec{b} \times \vec{c}).$$

Thus,

$$[DEGF] = \frac{1}{2} \cdot \frac{16}{35} |\vec{b} \times \vec{c}| = \frac{8}{35} \cdot 2730 \sin \theta = 624 \sin \theta.$$

Given

$$[DEGF] = 288,$$

we obtain

$$\sin \theta = \frac{288}{624} = \frac{6}{13}.$$

#### Step 6: Area of triangle $ABC$

$$[\triangle ABC] = \frac{1}{2} \cdot 30 \cdot 91 \cdot \sin \theta = 1365 \cdot \frac{6}{13} = 630.$$

#### Conclusion

The remaining task is to express the area of heptagon  $AFNBCEM$  in terms of the area of triangle  $ABC$ , using reflections about points  $F$  and  $E$ .

#### A.3 Phase 1: Truncation Points

We detect the potential collapse and truncate the erroneous trajectory at three distinct milestones  $(t_1, t_2, t_3)$ .

- **Truncation Point 1 ( $t_1$ ):**

We are given:

- Points  $D, E$  on  $AB$  such that  $AD < AE < AB$ ,
- Points  $F, G$  on  $AC$  such that  $AF < AG < AC$ ,
- Lengths:
  - \*  $AD = 4$
  - \*  $DE = 16$
  - \*  $EB = 8$
  - \*  $AF = 13$
  - \*  $FG = 52$
  - \*  $GC = 26$

- $M$  is the reflection of  $D$  through  $F$ ,
- $N$  is the reflection of  $G$  through  $E$ ,
- Area of quadrilateral  $DEGF = 288$ ,
- We are to find the area of heptagon  $AFNBCEM$ .

#### Step 1:

- **Truncation Point 2 ( $t_2$ ):**

We are given:

- Points  $D, E$  on  $AB$  such that  $AD < AE < AB$ ,
- Points  $F, G$  on  $AC$  such that  $AF < AG < AC$ ,
- Lengths:
  - \*  $AD = 4$
  - \*  $DE = 16$
  - \*  $EB = 8$
  - \*  $AF = 13$
  - \*  $FG = 52$
  - \*  $GC = 26$

- $M$  is the reflection of  $D$  through  $F$ ,
- $N$  is the reflection of  $G$  through  $E$ ,
- Area of quadrilateral  $DEGF = 288$ ,
- We are to find the area of heptagon  $AFNBCEM$ .

### Step 1: Understand the given structure

On  $AB$ :

$$AD = 4, \quad DE = 16, \quad EB = 8$$

$$AB = AD + DE + EB = 4 + 16 + 8 = 30$$

On  $AC$ :

$$AF = 13, \quad FG = 52, \quad GC = 26$$

$$AC = AF + FG + GC = 13 + 52 + 26 = 91$$

### Step 2:

#### • Truncation Point 3 ( $t_3$ ):

We are given:

- Points  $D, E$  on  $AB$  such that  $AD < AE < AB$ ,
- Points  $F, G$  on  $AC$  such that  $AF < AG < AC$ ,
- Lengths:
  - \*  $AD = 4$
  - \*  $DE = 16$
  - \*  $EB = 8$
  - \*  $AF = 13$
  - \*  $FG = 52$
  - \*  $GC = 26$
- $M$  is the reflection of  $D$  through  $F$ ,
- $N$  is the reflection of  $G$  through  $E$ ,
- Area of quadrilateral  $DEGF = 288$ ,
- We are to find the area of heptagon  $AFNBCEM$ .

### Step 1: Understand the given structure

On  $AB$ :

$$AB = 4 + 16 + 8 = 30$$

On  $AC$ :

$$AC = 13 + 52 + 26 = 91$$

### Step 2: Understand points $M$ and $N$

- $M$  is the reflection of  $D$  through  $F$ , so  $F$  is the midpoint of  $DM$ .

- $N$  is the reflection of  $G$  through  $E$ , so  $E$  is the midpoint of  $GN$ .

Since  $D$  lies on  $AB$  and  $F$  lies on  $AC$ , the reflection is a point reflection in the plane, not along a line.

We are asked to compute the area of the heptagon:

$$AFNBCEM$$

### Step 3:

## A.4 Phase 2: Micro-SVD & Probe Selection (At Truncation Point $t_1$ )

Here we detail the geometric intervention at the first truncation point.

### A.4.1 Manifold Estimation (Monte Carlo Samples)

Taking truncation point 1 as an example, the Teacher generates  $N$  look-ahead paths to estimate the local covariance matrix  $\Sigma_{t_1}$ . Note how these samples are semantically similar (confirming the Bias Manifold).

*MC Sample 1:* Understand the configuration. We have triangle

*MC Sample 2:* Understand the configuration. We have triangle

*MC Sample 3:* Understand the configuration. We have triangle

*MC Sample 4:* Understand and use given lengths. We

*MC Sample 5:* Understand the configuration. We are dealing with

*MC Sample 6:* Understand the configuration. We have triangle

*MC Sample 7:* Understand the configuration. We have triangle

*MC Sample 8:* Understand the configuration. Let's first sketch

#### A.4.2 Student Probe Candidates ( $L = 8$ tokens)

The Student model ( $\pi_\phi$ ) generates 8 candidate sequences. We calculate the **Orthogonality Score** for each relative to the Teacher’s estimated manifold.

*MC Sample 1:* Find  $AE, AB, AC$ . Orthogonality Score: 0.9403

*MC Sample 2:* Let  $A(x_1)$ . Orthogonality Score: 0.9844

*MC Sample 3:* Let  $A = (0)$ . Orthogonality Score: 0.9802

*MC Sample 4:* First, let’s find the Orthogonality Score: 0.7196

*MC Sample 5:* Let  $A = (0)$ . Orthogonality Score: 0.9801

*MC Sample 6:* We are given the lengths  $AD$ . Orthogonality Score: 0.8500

*MC Sample 7:* We know  $AB = AD +$ . Orthogonality Score: 0.9643

*MC Sample 8:* Since  $AD = 4, \dots$  Orthogonality Score: 0.9724

## B Reasoning Collapse Evidence

To verify the universality of the observed geometric pathology, we extended our spectral analysis to models of varying scales, specifically Qwen3-8B([Team, 2025b](#)) and QwQ-32B([Team, 2025c](#)). Employing the identical methodology on the AIME 2025 benchmark, we tracked the effective rank dynamics of the hidden state covariance matrices during inference. As illustrated in Figure 8 and Figure 9, both models exhibit a consistent pattern of spectral degeneration: despite their increased parameter counts, the effective rank decays significantly as the reasoning chain lengthens and enters erroneous loops. This evidence suggests that reasoning collapse is a fundamental geometric phenomenon that persists across model scales, rather than an artifact specific to smaller architectures.

## C Ablation Studies and Robustness Analysis

### C.1 Ablation Studies

To rigorously evaluate the contribution of each component in the Spectral Orthogonal Exploration (SOE) framework, we conduct ablation studies focusing on the necessity of the probe injection and

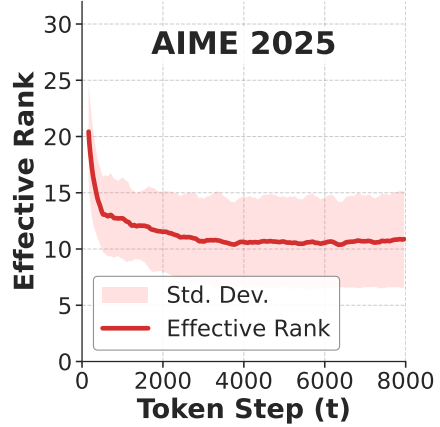


Figure 8: Reasoning Collapse of 8B Model

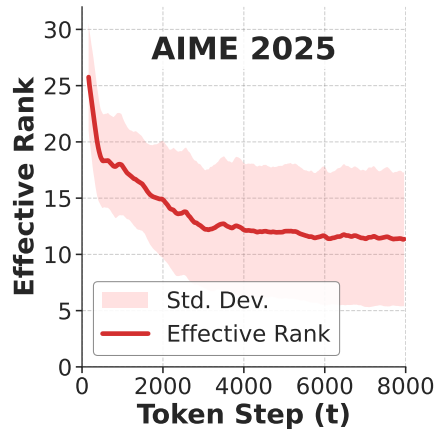


Figure 9: Reasoning Collapse of 32B Model

the effectiveness of the geometric selection mechanism. Due to computational resource constraints, these analyses were performed on the AIME 2025 benchmark.

**Validity of the Baseline as an Ablation.** We first emphasize that the **Baseline (Self-Consistency)** reported in the main text serves as the fundamental ablation of our framework. It represents the "No Injection" setting, where the Teacher model samples repeatedly from the same collapsed trajectory without any external intervention. The significant performance gap between the Baseline and SOE (as shown in the main results) confirms the essential value of the "Student Guides Teacher" paradigm.

**Effectiveness of Micro-SVD Selection (Random vs. Orthogonal).** To isolate the impact of our *Orthogonal Latent Stitching* (Micro-SVD) mechanism, we conducted a further ablation. In this setting, the Student generates candidate probes, but instead of selecting the candidate with the highest orthogonality score, we select one **at random** to

stitch into the Teacher’s context.

This comparison allows us to determine whether performance gains arise merely from adding “noise” (random perturbation) or from the specific geometric directionality of our method. As shown in Table 3, while random injection provides a performance boost over the baseline (58.82% vs 35.29%) by disrupting the bias manifold, our proposed SOE method achieves a significantly higher accuracy (70.59%). This result confirms that the Micro-SVD mechanism effectively identifies high-value directions in the Null Space that are superior to random perturbations.

Method	Pass@16 (AIME 25)
Baseline	35.29%
Ablation	58.82%
<b>Ours (SOE)</b>	<b>70.59%</b>

Table 3: Ablation study on AIME 2025. “Random Probe” indicates selecting a Student trace without geometric filtering. The results demonstrate that while any external diversity helps, directed orthogonal exploration yields the optimal performance.

**Sampling Efficiency.** Figure 10 further illustrates the sampling efficiency comparison. Our method reaches high-confidence solutions with fewer samples compared to both the Baseline and the Random Ablation, indicating that SOE navigates the solution space more efficiently.

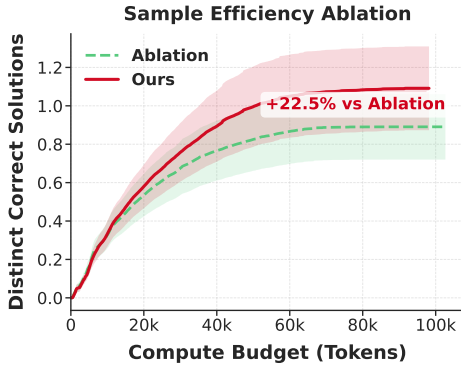


Figure 10: Sampling efficiency comparison between Baseline, Random Ablation, and SOE on AIME 2025. SOE discovers correct solutions at a significantly faster rate.

## C.2 Robustness Analysis

To evaluate the stability of our method against stochastic variations, we conducted repeated experiments on the AIME 2025 benchmark using three

distinct random seeds ( $\{42, 1024, 2024\}$ ). Due to computational resource constraints, this robustness analysis was restricted to the AIME 2025 dataset. As shown in Table 4, our method (SOE) consistently outperforms the baseline across all random seeds, demonstrating that the performance improvements are not artifacts of a specific initialization. Notably, while the baseline fluctuates between 29.41% and 41.18%, our method achieves a stable accuracy of up to 70.59%.

Seed	Baseline	Ours (SOE)
42	29.41%	64.71%
1024	41.18%	70.59%
2024	35.29%	70.59%

Table 4: Robustness analysis on AIME 2025 across three different random seeds. Our method demonstrates consistent performance gains despite stochastic variations.

## D Theoretical Proofs and Extended Analysis

### D.1 Proof of Proposition 1 and Analysis of Non-Linearity

*Proof.* Consider a simplified linear attention head. The output for a query  $q$  is given by:

$$\text{Attn}(q, K, V) = \sum_{i=1}^N \text{softmax}(q^T k_i) v_i \quad (9)$$

where  $v_i = W_V h_i$ . Since each input  $h_i \in \mathcal{S}$ , then each value vector  $v_i \in W_V \mathcal{S}$ . The output is a convex combination of vectors in  $W_V \mathcal{S}$ . Thus, the generated token embedding lies strictly in the span of the existing history. Without external noise or non-linearity capable of “folding” space into new dimensions, the model cannot access the Null Space  $\mathcal{S}^\perp$ .  $\square$

**Remark 1: The Inadequacy of Pointwise Non-Linearity.** A natural counter-argument suggests that the Feed-Forward Networks (FFNs) in Transformers, which contain non-linear activation functions (such as GELU, ReLU), might restore the lost dimensionality. We formally refute this by examining the coordinate-wise nature of these activations.

Consider the FFN update:  $h' = W_2 \sigma(W_1 h)$ . The linear transformations  $W_1, W_2$  can at most preserve the rank of the input:  $\text{rank}(W h) \leq \text{rank}(h)$ . Thus, any potential rank restoration relies solely on the non-linearity  $\sigma(\cdot)$ .

However, standard activation functions are **coordinate-wise**:  $\sigma(v)_i = \sigma(v_i)$ . They operate on each dimension independently without mixing information.

- **Zero-Variance Persistence:** If the input distribution has collapsed such that variance is zero along a basis vector  $e_j$  (i.e., the hidden states never "visit" this dimension), then for any sample  $h$ , the  $j$ -th component is constant (or zero). Since  $\sigma$  acts independently, the output  $\sigma(h_j)$  remains constant. The activation cannot spontaneously "light up" a dark dimension.
- **Manifold Curvature vs. Expansion:** While non-linearity can bend a flat  $k$ -dimensional subspace into a curved  $k$ -dimensional manifold, it does not increase the *intrinsic dimensionality*. A piece of paper crumpled into a ball (non-linear transformation) still has a surface area of dimension 2; it does not acquire volume.

Consequently, without an orthogonal external force (like our proposed injection), the FFN merely warps the collapsed Bias Manifold but remains topologically confined within it (Geva et al., 2021).

## D.2 Proof of Theorem 2

*Proof.* Let the attention weights be  $A \in \mathbb{R}^{N \times N}$ . The update rule roughly follows  $H_{t+1} = AH_t$ .

In the later stages of reasoning, the model often exhibits "confirmation bias," where tokens attend heavily to a few "anchor" tokens (e.g., repeating a premise). Mathematically, the Softmax distribution becomes sparse (approaching a Dirac delta). This reduces the effective number of basis vectors contributing to the output.

From the inequality of singular values  $\sigma_i(XY) \leq \|X\|\sigma_i(Y)$ , if the attention matrix  $A$  becomes effectively low-rank (due to sparse attention), then:

$$\text{rank}(H_{t+1}) \leq \min(\text{rank}(A), \text{rank}(H_t)) \quad (10)$$

□

## D.3 Semantic Sparsity Analysis

Here we discuss the informational contribution of the injection. Let the injected Student sequence be  $s_{inj}$  with length  $L_{inj}$  (8 tokens in our experiments), and the Teacher's context length be  $L_{ctx}$  (8192 tokens in our experiments).

**Argument: Semantic Sparsity.** The informational contribution of the injection to the global context mean is negligible:

$$\Delta\mu \approx \frac{L_{inj}}{L_{ctx}}(h_{Student} - \mu_{Teacher}) \approx 0 \quad (11)$$

Since  $L_{inj} \ll L_{ctx}$ , the "knowledge" impact on the centroid of the attention mechanism is minimal. This supports our claim that the Student is not "teaching" the Teacher via information transfer.

## E LLM Usage Statement

Large Language Models (LLMs) such as ChatGPT and Gemini were used as general-purpose writing assistants to improve readability and clarity of the manuscript (e.g., grammar checking, LaTeX formatting, and sentence restructuring). LLMs were not used to determine the research idea, perform literature search or generate the paper's key insights and conclusions. All analyses and conclusions are solely those of the authors.